Soft Matter

ARTICLE TYPE

Cite this: DOI: 00.0000/xxxxxxxxxx

Probing Wrapping Dynamics of Spherical Nanoparticles by 3D Vesicles Using Force-based Simulations†

Didarul Ahasan Redwan,[a] Ke Du[b], and Xin Yong*[a]

Received Date
Accepted Date

DOI: 00.0000/xxxxxxxxxx

Nanoparticles present in various environments can interact with living organisms, potentially leading to deleterious effects. Understanding how these nanoparticles interact with cell membranes is crucial for rational assessment of their impact on diverse biological processes. While previous research has explored particle–membrane interactions, the dynamic processes of particle wrapping by fluid vesicles remain incompletely understood. In this study, we introduce a force-based, continuum-scale model utilizing triangulated mesh representation and discrete differential geometry to investigate particle–vesicle interaction dynamics. Our model captures the transformation of cell membrane shapes and nanoparticle wrapping by calculating the forces arising from membrane bending energy and particle adhesion energy. The simulation is validated through comparisons with theoretically predicted minimal bending energy and corresponding vesicle shapes. We then examine the interactions between spherical vesicles and individual nanospheres, both externally and internally, and quantify energy landscapes across different wrapping fractions of the nanoparticles. Furthermore, we explore multiple particle interactions with biologically relevant fluid vesicles with nonspherical shapes. Our study reveals that initial particle positions and interaction sequences are critical in determining the final equilibrium shapes of the vesicle–particle complex in these interactions. These findings emphasize the importance of nanoparticle positioning and wrapping fractions in the dynamics of particle–vesicle interactions, providing crucial insights for future research in the field.

1 Introduction

Recent advancements in nanotechnology have sparked significant interest in the interactions between living organisms and nanoparticles produced from primary and secondary sources[6,20,36]. Metal and polymer nanoparticles are particularly promising in biomedical research for drug delivery, offering advantages such as targeted delivery and controlled release of therapeutic agents[19,20,29,55,65]. Despite these potential benefits, there are growing concerns about the safety of engineered and industrial nanoparticles directly released into the environment. The term "nanotoxicity" refers to the possible harmful effects of nanoparticles on living organisms and represents a significant concern due to their wide range of applications[43–45,51,69]. Besides those from primary sources, trillions per liter of secondary nanoparticles can be generated from common consumer plastic produces during normal use and many more are produced by environmental degradation of enormous plastic waste[30,76]. Given this concern, there has been a surge in efforts to elucidate how nanoparticles interact with biomembranes and living cells[1,3,4,73,78]. Investigating the intricate dynamics of cellular nanoparticle uptake has been a subject of extensive experimental interest, as evidenced by notable studies[10,23,31,70,80]. Yet, direct observation remains challenging due to the complexity of these interactions and inherent technical constraints. Hence, computational simulations have emerged as a promising tool, shedding light on dynamic processes like nanoparticle encapsulation by cellular membranes[4,5,53,74,75]. In this study, we utilize computational modeling to reveal the intricate dynamics governing the interactions between spherical nanoparticles and three-dimensional (3D) fluid vesicles.

The cell membrane, a lipid bilayer, acts as a selectively permeable barrier that separates the cell from its external environment. For nanoparticles to enter or exit the cell, they must traverse this barrier[14,16]. Nanoparticle transport modes can be classified into direct penetration through passive diffusion and active translocation based on particle size. Small hydrophobic nanoparticles with sizes of a few nanometers can penetrate the membrane directly via thermal diffusion. Oppositely, particles significantly larger than the membrane thickness resort to energy-intensive transport processes such as endocytosis and exocytosis.

[a] Department of Mechanical Engineering, Binghamton University, Binghamton, New York 13902, United States. E-mail: xyong@binghamton.edu
[b] Department of Chemical and Environmental Engineering, University of California Riverside, Riverside, California 92521, United States.

† Electronic Supplementary Information (ESI) available: [details of any supplementary information available should be included here]. See DOI: 10.1039/cXsm00000x/

https://doi.org/10.26434/chemrxiv-2023-wrgnr **ORCID:** https://orcid.org/0000-0002-8894-2750 Content not peer-reviewed by ChemRxiv. **License:** CC BY-NC-ND 4.0

During these processes, the membrane substantially deforms and engulfs around the nanoparticles[9,22,27,73]. Spontaneous wrapping is initiated when the adhesive energy between the nanoparticle and the membrane outweighs the energy penalty associated with bending the membrane to wrap the particle[4]. Continuum-scale models based on Helfrich theory[35] and dynamic triangulated surfaces[26,33,41,48,49,52] have been predominantly employed to describe cell membrane elasticity and study the interactions of fluid vesicles with nanoparticles. Notably, Bahrami *et al.*[3] as well as Saric and Cacciuto[60] pioneered the investigation of vesicle tabulation triggered by nanoparticle adsorption and ensuing nanoparticle aggregation. These models were later extended to study the wrapping of particles with anisotropic shapes, including ellipsoids, rods, and cuboids[2,17,18], as well as those with heterogeneous surface chemistry[5].

Recently, modeling studies have expanded to reveal the effects of vesicle properties. Yu *et al.*[75] investigated interactions between nanoparticles and vesicles with different shapes (stomatocytes, prolates, and oblates), systematically characterizing the effects of vesicle volume and membrane curvature on particle wrapping. They also examined cuboid particles and biconcave vesicles to identify the energy-minimized shapes of these vesicles. The same group further predicted phase diagrams for spherical nanoparticles wrapped by vesicles with varying osmotic pressure[74]. Their findings elucidated that the energy barrier of discontinuous envelopment transition increases with increasing osmotic concentration, stabilizing partially wrapped states. Another recent study by Sadhu *et al.*[56] modeled the effect of curvature-inducing proteins on the engulfment of a rigid spherical particle via the Metropolis Monte Carlo algorithm. Their study demonstrated proteins with concave shapes can augment the wrapping process by decreasing the bending energy cost of the membrane and adhering the particle to the surface.

While existing research offers valuable insights into the final equilibrium states of particle–vesicle systems, they predominantly rely on energy minimization techniques[53,56]. In the context of membrane shape optimization, energy minimization involves iteratively adjusting the shape of the membrane to find a configuration where the potential energy of the system is minimized. A considerable shortcoming of these energy-centric methods is their inability to explicitly depict the dynamics of particle interactions and membrane deformations[56]. To probe interaction dynamics, particle-based methods such as molecular dynamics and dissipative particle dynamics are often employed[59,72,73]. Nonetheless, these simulations suffer from limitations in temporal and spatial scales[37,71], hindering their ability to model the wrapping dynamics on a cellular scale. To bridge this gap, we built a computational framework using triangulated membrane representation and discrete differential geometry to compute forces acting on membrane and particle and accurately simulate the nanoparticle wrapping dynamics by fluid vesicles.

In this study, our initial step was to validate the numerical method by predicting the shape transformations of fluid vesicles. Subsequently, we simulated the dynamics of a single-particle interaction and wrapping by a spherical fluid vesicle, delving into the interaction energy landscapes and induced shape changes. Both external and internal nanoparticle wrapping processes were examined quantitatively. We further investigated how two initially distant nanoparticles interact with the vesicle, characterizing the energy profiles and the evolution of particle configurations driven by membrane-mediated interactions. Finally, aiming to model biologically relevant uptake, we analyzed the impact of nanoparticle positioning during the wrapping process as they interacted with a biconcave-shaped vesicle, a shape reminiscent of a red blood cell.

2 Theoretical Background and Simulation Setup

2.1 Membrane elasticity theory

The continuum theory of membrane elasticity describes the deformation of a lipid bilayer membrane using the Helfrich-Canham-Evans Hamiltonian (referred to as the Helfrich Hamiltonian below)[13,24,32,35]. The membrane is considered a curved two-dimensional (2D) surface embedded in three-dimensional (3D) space, which exhibits fluid-like behaviors in the plane of the membrane while resisting stretching and bending. The fluidity of biological membranes is attributed to the lateral diffusivity of lipid molecules within the lipid bilayer. The membrane does not contain any memory of the previous shape or configuration, indicating the energy functional is solely dependent on the current geometry[21]. The bending free energy of the membrane can be expressed as a functional of mean curvature (H), spontaneous mean curvature (H_0), and Gaussian curvature (G) as follows[50]:

$$E_b = \oint dA \left\{ 2\kappa_b (H - H_0)^2 + \kappa_G G \right\} \tag{1}$$

Here, $H = (c_1 + c_2)/2$ and $G = c_1 \cdot c_2$ with c_1 and c_2 representing two principal curvatures. The spontaneous mean curvature H_0 can be influenced by various factors, including embedded proteins and lipid composition asymmetry between the two leaflets. The local elastic properties of the membrane are described by κ_b and κ_G, which represent the bending and Gaussian curvature moduli, respectively. When there is no change in the membrane topology, the Gaussian curvature term can be neglected because the corresponding surface integral remains constant according to the Gauss-Bonnet theorem[15,46]. The minimization of the Helfrich Hamiltonian thus results in a fourth-order nonlinear partial differential equation that describes the optimized shape of the membrane possessing the lowest bending energy. However, this formidable "shape" equation has only been solved analytically for a limited number of highly symmetric cases[64].

Besides the bending energy, the physical models for 3D vesicles also often include the contributions from surface tension energy (E_a) and osmotic pressure energy (E_v). The area energy can be expressed by the following equation[11,64]:

$$E_a = \kappa_a \frac{(A - A_0)^2}{A_0} \tag{2}$$

Here, A_t and A_0 represent the current and preferred total areas of the membrane, respectively. κ_a is the area expansion modulus that controls the strength of penalty to maintain a preferred vesicle area[67], which can also be interpreted as a Lagrange multiplier that helps to fix the total area. A closed membrane also regulates

https://doi.org/10.26434/chemrxiv-2023-wrgnr **ORCID:** https://orcid.org/0000-0002-8894-2750 Content not peer-reviewed by ChemRxiv. **License:** CC BY-NC-ND 4.0

the enclosed volume accordingly. Therefore, we consider a volume energy of the vesicle as [11,28,64]:

$$E_v = \kappa_v \frac{(V - V_0)^2}{V_0} \tag{3}$$

Here, V and V_0 denote the current and preferred volumes enclosed by the membrane, respectively. The volume constraint modulus, denoted by κ_v, acts as a control parameter that influences how strongly the system penalizes deviations from the desired volume [62]. The volume control term can also be interpreted as the contribution of osmotic pressure when the system is close to the isosmotic condition [74,81]. Thus, the total energy of the vesicle is composed as follows:

$$E_{vesicle} = E_b + E_a + E_v \tag{4}$$

2.2 Calculation of discrete geometric properties

Due to the challenging math involved in solving the shape equation, an alternative approach to the problem of membrane shape optimization is to discretize a smooth surface into a triangulated mesh. Discrete differential geometry [34] is used to calculate the surface geometric quantities necessary for computing the energy functional. We convert a 2D surface M into a triangular mesh network. The mesh consists of vertices V, edges E, and triangles T. Each vertex $v_i \in V$ represents a point on the original surface, and its 3D coordinates determine the shape of the surface. Each triangular element $t_i \in T$ is defined by a group of 3 vertices $(v_i, v_j, v_k) \in V$ sharing a common triangle. In order to compute the bending energy and force, it is necessary to determine the curvatures and surface normal at each vertex of the triangulated surface. Meyer *et al.* [47] proposed a method to define surface geometric properties at discrete mesh vertices as spatial averages. The averaging process is performed within the immediate neighboring triangles, referred to as the "1-ring neighborhood". Figure 1 provides a schematic representation of the 1-ring neighborhood surrounding a particular vertex i with its position given by a vector $\mathbf{x}_i$. Meyer *et al.* [47] introduced a mixed vertex area to ensure the proper tiling of the surface area in the presence of obtuse triangles to minimize the error originating from spatial averaging.

The mean curvature of a 2D smooth surface is related to its Laplacian at position $\mathbf{x}$ by the following equation:

$$\Delta_s \mathbf{x} = 2H\mathbf{n} \tag{5}$$

Here, $\mathbf{n}$ is the unit outward normal vector of the surface. Thus, the discrete mean curvature $H(\mathbf{x}_i)$ at a vertex i can be calculated by the cotangent formula:

$$H(\mathbf{x}_i) = |\mathbf{K}(\mathbf{x}_i)| = \frac{1}{4A^i_{\text{mixed}}} \left| \sum_j^{N_v(v_i)} (\cot\alpha_{ij} + \cot\beta_{ij})(\mathbf{x}_i - \mathbf{x}_j) \right| \tag{6}$$

Here, α_{ij} and β_{ij} respectively correspond to the angles opposite to edge $(\mathbf{x}_i, \mathbf{x}_j)$, and $N_v(v_i)$ is the set of 1-ring neighbor vertices of i. The sign of the mean curvature H is determined by whether the direction of the outward normal vector $\mathbf{n}(\mathbf{x}_i)$ matches the sign of the mean curvature vector $\mathbf{K}(\mathbf{x}_i)$ at vertex i. $\mathbf{n}(\mathbf{x}_i)$ can be calculated by the "mean weighted angle" approach [39]. When the signs are the same, the mean curvature is considered positive; otherwise, it is regarded as negative. The discrete Gaussian curvature $G(\mathbf{x}_i)$ can be obtained as a vertex angular deficit by employing the discrete version of the Gauss-Bonnet theorem [40,46]:

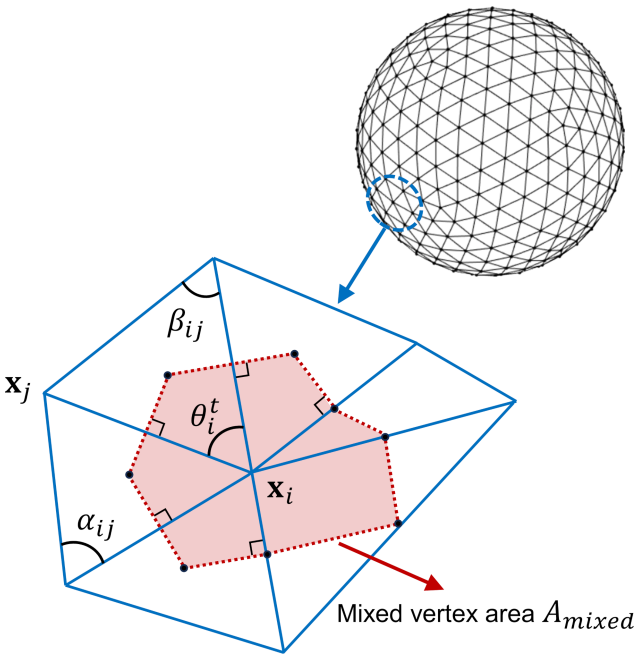

Fig. 1 Schematic diagram of a spherical vesicle mesh and the 1-ring neighborhood of a vertex. The shaded region enclosed by the dashed lines represents the mixed vertex area A_{mixed}.

$$G(\mathbf{x}_i) = \frac{1}{A^i_{mixed}} \left(2\pi - \sum_t^{N_t(v_i)} \theta_i^t \right) \tag{7}$$

with θ_i^t representing the angle at vertex i in triangle t. $N_t(v_i)$ is the set of 1-ring neighbor triangles of v_i.

The total volume of the vesicle can be defined as $V = \sum_t^{N_t} V^t$, where V^t is the volume of the tetrahedron formed by a triangle and an arbitrary point (selected as the origin here) and N_t is the total number of triangles of the mesh. This volume is calculated by the following formula [15]:

$$V^t = \frac{1}{3} A^t h \tag{8}$$

Here, A^t is the area of the triangle and h is the corresponding height of the tetrahedron. The total area of the membrane surface is computed by summing up areas of all triangles:

$$A = \sum_t^{N_t} A^t \tag{9}$$

Detailed benchmarks of numerical calculations of the mean curvature and the Laplacian of the mean curvature can be found in Section 1 of the Electronic Supplementary Information (ESI) (also see Figures S1 and S2)

https://doi.org/10.26434/chemrxiv-2023-wrgnr **ORCID:** https://orcid.org/0000-0002-8894-2750 Content not peer-reviewed by ChemRxiv. **License:** CC BY-NC-ND 4.0

2.3 Forces on discretized surface

The bending force acting on each vertex of the triangular mesh can be calculated from the force density vector $\mathbf{f}$, which is given by the first variation of the bending energy functional[42,66,79]

$$\mathbf{f} = 2\kappa_b \left[2(H-H_0)(H^2+H_0H-G)+\Delta_s H\right]\mathbf{n} \tag{10}$$

Here, $\Delta_s H$ denotes the Laplacian of the mean curvature, which again can be calculated by the cotangent expression on discretized surfaces. The nodal bending force is then calculated by multiplying the mixed vertex area with the force density vector evaluated at vertex i

$$\mathbf{f}_b = \mathbf{f}(\mathbf{x}_i)A^i_{mixed} \tag{11}$$

The area constraint force is calculated by taking the negative positional gradient of the energy:[25,81]:

$$\mathbf{f}_a = -\frac{\partial E_a}{\partial \mathbf{x}_i} = -\kappa_a \frac{2(A-A_0)}{A_0}\sum_t^{N_t}\frac{\partial A^t}{\partial \mathbf{x}_i} \tag{12}$$

The discretized form of the area gradient for vertex i is described below[11]:

$$\sum_t^{N_t}\frac{\partial A^t}{\partial \mathbf{x}_i} = \frac{1}{2}\sum_j^{N_v(v_i)}(\cot\alpha_{ij}+\cot\beta_{ij})(\mathbf{x}_i-\mathbf{x}_j) \tag{13}$$

Similarly, the force derived from the volume constraint can be calculated by using the following equations[11,81]:

$$\mathbf{f}_v = -\frac{\partial E_v}{\partial \mathbf{x}_i} = -\kappa_v \frac{2(V-V_0)}{V_0}\sum_t^{N_t}\frac{\partial V^t}{\partial \mathbf{x}_i} \tag{14}$$

Here, the volume gradient term can be obtained by the following expression[11]:

$$\sum_t^{N_t}\frac{\partial V^t}{\partial \mathbf{x}_i} = \frac{1}{3}\sum_t^{N_t} A^t\mathbf{n}^t \tag{15}$$

Here, $\mathbf{n}^t$ is unit face normal for each triangle A^t.

2.4 Membrane–particle interaction

The adhesion energy between the membrane surface and particle surface regulates the process of particle wrapping by a membrane. We can express the adhesion energy between the discretized surface and the particle as follows[2,3]:

$$E_{ad} = \sum_i^{N_v} V(d_i)A^i_{mixed} \tag{16}$$

Here, $V(d_i)$ is the particle–membrane interaction energy per unit area, which depends on the distance between the vesicle vertices and the surface of the particle $d_i = |\mathbf{x}_i - \mathbf{x}_0| - R_p$ with $\mathbf{x}_0$ representing the particle center and R_p denoting the particle radius. The interaction between particle and membrane can be attributed to electrostatic and van der Waals forces, as well as the binding of specific receptor and ligand molecules anchored in the membrane and on the particle surface. In this study, we model adhesion using a continuous Morse potential[1,53,54]

$$V_M(d_i) = U(e^{-2d_i/\rho} - 2e^{-d_i/\rho}) \tag{17}$$

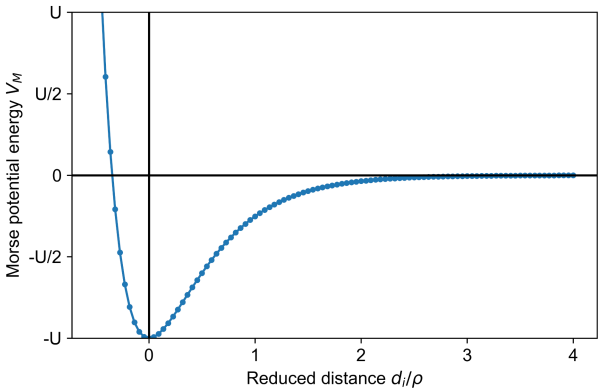

Fig. 2 Energy profile of the Morse potential.

which is characterized by its depth U and potential range ρ as shown in Figure 2. The potential takes the minimal value of $-U$ at $d_i = 0$, corresponding to the equilibrium distance between the particle and bound membrane patch. By comparing the adhesion energy to the bending energy, we can define a rescaled adhesion energy $u = UR_p^2/\kappa_b$, governed by bending modulus κ_b, adhesion energy density U, and particle radius R_p. $u = 2$ is the critical value at which the unwrapped and fully wrapped state of the particle theoretically have equal total energies[1]. Similar to other nodal forces, the adhesion force on each vertex is given by

$$\mathbf{f}_{ad} = -\frac{\partial E_{ad}}{\partial \mathbf{x}_i} \tag{18}$$

The total energy of the system including the contribution from the adhesion energy is

$$E_{total} = E_{vesicle} + E_{ad} \tag{19}$$

2.5 Time integrator and mesh regularization

The forward Euler method is a commonly used time integrator in numerical simulations, particularly when solving differential equations that govern the evolution of a system over time. It serves as a fundamental tool for advancing the solution in discrete time steps[61]. This explicit method is applied to update a system state. The total force ($\mathbf{f}_{total}$) of each vertex is calculated to obtain the vertex velocity ($\mathbf{v}$). The new vertex position is given for the following time step.

$$\mathbf{v} = \dot{\mathbf{x}} = \mathbf{f}_{total}/\gamma = (\mathbf{f}_b + \mathbf{f}_a + \mathbf{f}_v + \mathbf{f}_{ad})/\gamma \tag{20}$$

Here, γ is an effective drag coefficient representing the strength of viscous dissipation from the background, considering the vesicle is immersed in a liquid. In terms of optimization, the forward Euler scheme is equivalent to the gradient descent algorithm for minimizing an objective function, which herein is the discrete energy. Being a first-order approach, the accuracy of the integrator increases linearly as the time step size decreases. There is a trade-off between accuracy and efficiency, as smaller time increments also increase the computational cost of the simulation. Notably, the forward Euler method has some drawbacks despite its ease

https://doi.org/10.26434/chemrxiv-2023-wrgnr **ORCID:** https://orcid.org/0000-0002-8894-2750 Content not peer-reviewed by ChemRxiv. **License:** CC BY-NC-ND 4.0

of use. For instance, they may be unstable for simulations involving rigid systems or solutions that oscillate quickly. More sophisticated temporal integrators, such as the velocity-verlet or implicit methods, may be more suitable in certain circumstances. In simulations with multiple particles, the relative motion between particles during their interaction with the vesicle is of interest. Thus, the particle dynamics is modeled by simply calculating the reaction force ($\mathbf{f}_p$) of the adhesion force according to Newton's third law. Notably, different from $\mathbf{f}_{ad}$ which includes contributions from variations in both Morse potential and membrane vertex area (see Eqs. 16 and 18), the reaction force on the particle accounts for only the contribution from the adhesion potential. To prevent particle overlap, a linear excluded volume repulsion ($\mathbf{f}_{ev}$) is also introduced. The particle velocity ($\mathbf{v}_p$) is then calculated by $\mathbf{v}_p = (\mathbf{f}_p + \mathbf{f}_{ev})/\gamma_p$ with γ_p being the effective drag coefficient for nanoparticles.

We observed that the triangulated mesh configuration of the vesicle could suffer from significant distortions when interacting with particles, such as elongation in one direction or the generation of obtuse angles. In this force-based scheme, the nodal forces depend sensitively on the underlying mesh geometry. When the mesh structure deforms abruptly, the force variations can lead to numerical instability, convergence issues, or even divergence of the simulation. As a result, the system energy is also significantly affected by mesh quality. To improve simulation stability and ensure the accuracy of the energy analysis, two mesh regularization schemes are implemented. The first regularization scheme is the equiangulation[12], also known as the T2 bond flipping[33]. By using this method, we aim to optimize the triangular configurations of the mesh to achieve equilateral or near-equilateral triangles. The second regularization scheme is the "vertex averaging"[12] to redistribute the vertices to improve the mesh homogeneity. For each vertex, this operation computes a new position by taking the area-weighted average of the centroids of the triangles connected to the vertex. Both regularization schemes play crucial roles in preserving the quality of the triangulated mesh during its evolution. By mitigating mesh distortion and preserving uniform triangular elements, these techniques contribute to more reliable simulations of the particle–vesicle system.

Determining the geometric properties of the triangulated surface of the vesicle constitutes a pivotal component in the computation of force and energy terms. To increase computational efficiency, we utilized the libigl C++ library for the geometric calculations[38]. The simulations were performed by in-house C++ code.

3 Results and Discussion

3.1 Vesicle shape transformation

We performed a comprehensive validation of our model by reproducing previously observed phase diagrams of vesicle shapes. The initial vesicle shapes were selected as oblate and prolate spheroids. The bending modulus κ_b, volume modulus κ_v, and area modulus κ_a were set to 0.01, 2.0, and 1.0 respectively. The preferred surface area A_0 was set to the surface area of a unit sphere 4π. The preferred vesicle volume is calculated according to the reduced volume, which is the ratio of the vesicle volume V to the volume of a sphere with the same surface area A, $v = 6\sqrt{\pi}V/A^{3/2}$. Other simulation parameters are given in Table 1.

Table 1 Model parameters used for vesicle shape transformation and nanoparticle–vesicle interaction simulations

Parameters	Values
Spherical vesicle radius (R_v)	1.0
Spontaneous mean curvature (H_0)	0.0
Bending modulus (κ_b)	0.01
Area expansion modulus (κ_a)	1.0
Volume constraint modulus (κ_v)	0.0 (Spherical vesicles) or 2.0 (Biconcave vesicle)
Particle radius (R_p)	0.2-0.4
Rescaled adhesion energy (u)	2.0
Morse potential range (ρ)	0.01
Membrane drag coefficient (γ)	1.0
Particle drag coefficient (γ_p)	100.0
Time step (δt)	0.01

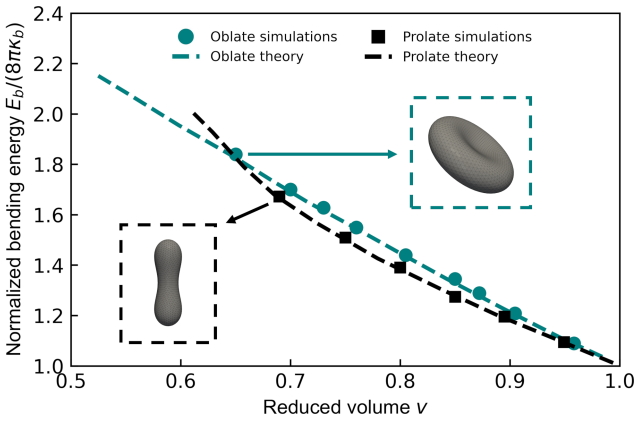

Fig. 3 Minimized energy states at different reduced volumes for vesicles with the oblate and prolate spheroids as the initial shapes. The number of triangles of the mesh is 5120. The dashed lines represent the theoretical results adapted from Ref.[63]. The insets show representative dumbbell and biconcave shapes of vesicles at low reduced volume.

Figure 3 presents the energy curves following different reduced volumes for initial oblate and prolate vesicle configurations. This diagram delineates the normalized bending energy of the vesicles in relation to the reduced volume. Notably, the phase diagram we derived from vesicle shape optimization aligns closely with theoretical predictions in both energy and shapes. Figure S3 in ESI showcases the final equilibrium shapes of both prolate and oblate branches for v ranging from 0.6 to 1.0. For the prolate branch, the vesicle elongates as the reduced volume decreases. When v reaches 0.67, the vesicle adopts a dumbbell shape. Further reductions in volume lead to the emergence of metastable states[11]. In contrast, vesicles initially shaped as oblates flatten as v decreases and transition to a biconcave form when the reduced volumes lie between 0.59 and 0.65. Crucially, it is observed that a single target reduced volume can yield two distinct, locally minimized energy states, contingent on the initial shape of the vesicle.

https://doi.org/10.26434/chemrxiv-2023-wrgnr **ORCID:** https://orcid.org/0000-0002-8894-2750 Content not peer-reviewed by ChemRxiv. **License:** CC BY-NC-ND 4.0

3.2 Interactions of single particles with spherical vesicles

Endocytosis and exocytosis are cellular processes involved in the transport of colloidal particles across cell membranes[57,58,68,77]. Endocytosis is the process by which a cell takes in substances from its surroundings. Exocytosis, on the other hand, helps the cell release substances into the external environment. To model these two processes, we explore the interaction of vesicles with external and internal particles. A sign convention is employed to differentiate between the particles located inside and outside the vesicle such that the relative curvature $C_r = \pm R_p/R_v = \pm R_p$ with $R_v = 1$. The positive and negative signs correspond to the particles outside and inside the vesicle, respectively. Due to the use of continuous Morse potential with a finite potential range, we introduce an effective wrapping fraction of the nanoparticles based on adhesion energy to quantify the wrapping state. Namely, it is defined by the ratio of the adhesion energy E_{ad} computed in the simulation to the theoretical adhesion energy corresponding to the wrapping of the entire particle, given as $\chi_{eff} = E_{ad}/\left(4\pi U R_p^2\right)$. The nanoparticle is fixed during the wrapping.

We examine the total and bending energies of the particle–vesicle system to gain quantitative insights into their interactions. The theory predicts significant energy barriers associated with the wrapping of external particles[4]. Therefore, to explore and sample states that are energetically unfavorable, we introduce a harmonic biasing potential, which resembles the ideas of umbrella sampling[7,8] used in molecular dynamics simulations. This potential adds a restraining force that assists in reaching target wrapping fractions.

Figure 4a plots the total equilibrium energies of the particle–vesicle complex at different wrapping fractions. The profiles exhibit distinct behaviors between internal and external particle wrapping. For external particles of $C_r = 0.3$ and 0.4, the total energy first increases and then decreases as χ_{eff} increases. The maximum corresponds to an energy barrier that inhibits spontaneous wrapping. However, if the energy barrier were overcome, the wrapping would proceed until membrane fission to complete the internalization of the fully wrapped particle (not incorporated in the present model). Interestingly, the profile for the $C_r = 0.2$ particle also shows a minimum around $\chi_{eff} = 0.2$ in contrast to the theoretical predictions[4], which suggests limited spontaneous wrapping of small external particles. This discrepancy is attributed to the effects of membrane surface discretization (discussed in detail below) and the interaction potential with a finite range. Oppositely, when particles interact with the membrane from the inside, the total energy monotonically decreases until an effective wrapping fraction of approximately 0.6 is reached, indicating spontaneous wrapping. This observation suggests that internal particles naturally affiliate with the membrane. However, additional energy is required to exceed the optimal degree of wrapping. Compared with external wrapping showing pronounced particle size effects, the wrapping of internal particles is significantly less sensitive to the relative curvature, evinced by the collapse of energy curves.

Figure 4b shows the variations in the bending energy of the vesicle induced by particle wrapping. When particles are not

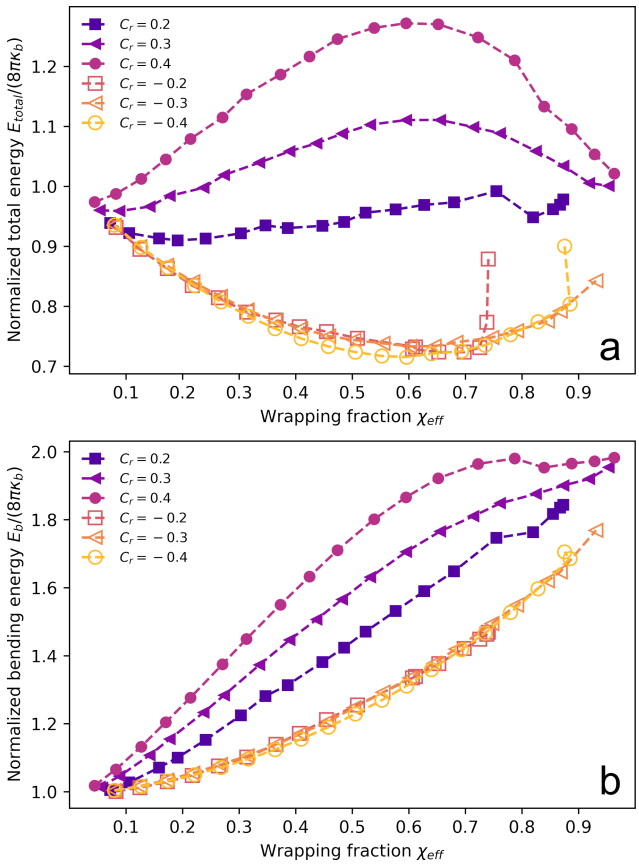

Fig. 4 Normalized (a) total and (b) bending energies as functions of effective wrapping fractions (χ_{eff}) and relative curvature (C_r) of the particles. C_r is positive for a particle outside the vesicle (closed markers) and negative for a particle inside the vesicle (open markers).

wrapped, the bending energies converge to that of an unaltered spherical vesicle, specifically $8\pi\kappa_b$. As the wrapping fraction increases, the bending energies rapidly increase due to the adhesion-induced vesicle deformation. As the wrapping fraction is close to 1.0, the bending energy approaches $16\pi\kappa_b$ regardless of the particle location. This limiting state corresponds to the full wrapping in which two spherical membrane patches are connected by an infinitesimal neck. Notably, external particles induce a steeper bending energy increase relative to those inside. Consistent with the total energy profiles, the particle size has a pronounced effect on external wrapping while the bending energy differences among internal particles are negligible. This observation underscores that external particles exert a more significant influence on vesicle deformation dynamics.

Figures S4 and S5 in the ESI showcase the vesicle morphology changes when interacting with external and internal particles, respectively. At low wrapping fractions, vesicles retain a nearly spherical shape. Yet, as χ_{eff} rises, specifically within the range from 0.3 to 0.7, the vesicle undergoes notable deformations both local to the particle as well as in the global shape due to the conservation of membrane area. Depending upon the particle location, the local deformations can adopt either concave or convex configurations. When wrapping a large external particle, the vesicle morphs into a distinct kidney-like shape. In contrast, the

https://doi.org/10.26434/chemrxiv-2023-wrgnr **ORCID:** https://orcid.org/0000-0002-8894-2750 Content not peer-reviewed by ChemRxiv. **License:** CC BY-NC-ND 4.0

vesicles interacting with internal particles predominantly evolve into teardrop shapes as wrapping progresses, consistent among different particle sizes. At $\chi_{eff} = 0.9$, the simulation snapshots clearly show the formation of a neck connecting the membrane patch wrapping the particle to the parent vesicle. Particularly in external wrapping, the neck region resembles a catenoid, an exemplary minimal surface with zero mean curvature and thus zero bending energy.

In Figure 4, it is evident that for the smallest particles of size 0.2 (highlighted by square markers), the systems cannot reach target wrapping fractions greater than 0.9 and 0.8 for external and internal wrapping, respectively. Moreover, the energy profiles exhibit anomalous variations at high wrapping fractions. We assert that this behavior is attributed to insufficient mesh resolutions to accurately capture the high curvature bending induced by the small particles. Thus, we conducted a mesh-sensitivity study to assess the influence of mesh density and particle size on the wrapping state. Our tests utilize a coarser mesh consisting of 5120 triangles and a finer mesh having 20480 triangles. Figure S6 demonstrates substantial deviations in both the bending and total energy profiles between the coarser and finer meshes. The finer mesh not only enables the simulation of higher effective wrapping fractions but also results in smoother variations in the energy profiles. However, for particles with a radius of 0.3 shown in Figure S7, the differences between the two meshes are much less discernible, suggesting the interaction is accurately captured. We also note that the total energy for external wrapping plateau at the extreme target wrapping fractions of 0.95, deviating from the further decrease predicted by the theory[1].

To further understand the mesh resolution effect, Figure S8 presents a visual sequence illustrating neck formation in a system with a high wrapping fraction around 0.9. Notably, an intermediate state where the membrane shape is still evolving features an unstable neck morphology, as shown in Figures S8a,b. Theoretically, the neck radius would shrink asymptotically to zero (corresponds to the membrane fission) as the wrapping fraction approaches 1.0. The triangulated surface will inevitably fail to accurately represent the small neck with high curvature, resulting in an overestimation of the mean curvature and bending energy. Consequently, the neck expands unphysically to relieve the excess bending energy as shown in Figures S8c,d, leading to the reduction in the effective wrapping fraction. These findings shed light on the intricate evolution of vesicle morphology in response to particle introduction, further elucidating the interplay between particle size, curvature, and resulting vesicle shapes. Despite external wrapping at extreme wrapping fractions, the interactions of nanoparticles of radius 0.3 are accurately modeled. Thus, we focus on this particle size in the following simulations.

3.3 Interactions of two particles with spherical vesicles

In this section, we delve into the dynamics of a spherical vesicle concurrently interacting with two nanoparticles, each with a size parameter of $C_r = 0.3$ at different wrapping fractions. We consider relative particle motion to efficiently probe the interaction dynamics, as described in Section 2.5. As in our previous analyses, we employ the umbrella potential to explore states that are energetically less favorable. Our findings reveal that when a vesicle interacts with two particles, the resulting equilibrium energy profiles (both total and bending) resemble those for the single-particle interactions, as detailed in Figures 5a,b. The bending energies of both external and internal wrapping are significantly higher because the vesicle has to deform more to accommodate extra particles. Compared to a single particle, the external wrapping of two particles needs to overcome a higher energy barrier, while the wrapping of two inside particles is energetically more favorable. Notably, both the minimum and maximum of the total interaction energy are located at χ_{eff} of approximately 0.7, slightly higher than in the single-particle interactions.

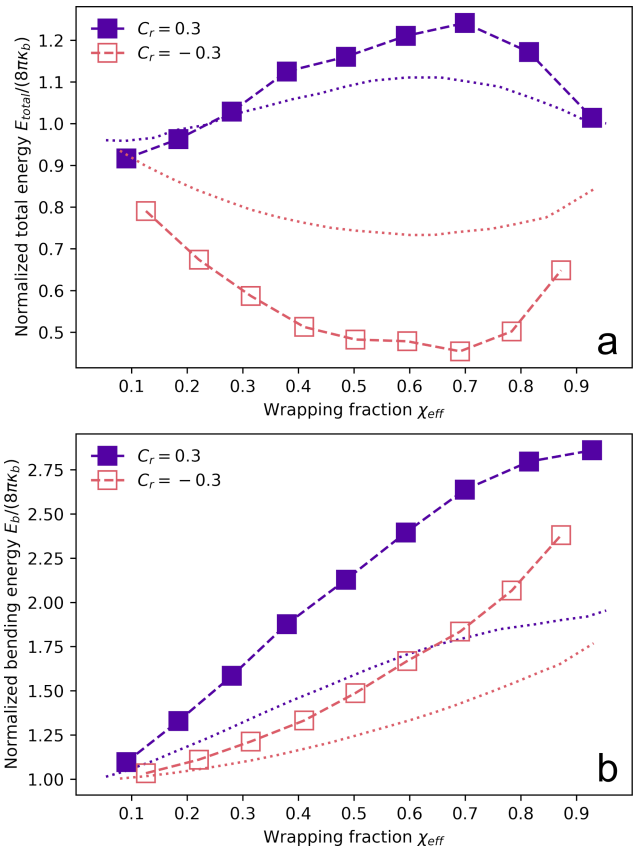

Fig. 5 Normalized (a) total and (b) bending energies of spherical vesicles interacting with two nanoparticles having a relative curvature of 0.3 at different effective wrapping fractions. The solid and open markers represent the states with particles located outside and inside of the vesicle, respectively. Dotted lines present the energy profiles for the corresponding single-particle interaction for comparison.

We quantify the distances between the two particles as they interact and become wrapped by the vesicle. As shown in Figure 6, for particles within the vesicle, the interparticle distance (d_p) increases proportionally with the increasing wrapping fraction. Concurrently, there is a noticeable elongation of the vesicle, with the particles positioning themselves at opposite poles. Oppositely, during external wrapping, d_p decreases monotonically. Initially, at low wrapping degrees ($0 \leq \chi_{eff} \leq 0.5$), the vesicle appears squeezed by the particles due to the wrapping. However, as the wrapping fraction exceeds 0.5, the vesicle tends to revert

https://doi.org/10.26434/chemrxiv-2023-wrgnr **ORCID:** https://orcid.org/0000-0002-8894-2750 Content not peer-reviewed by ChemRxiv. **License:** CC BY-NC-ND 4.0

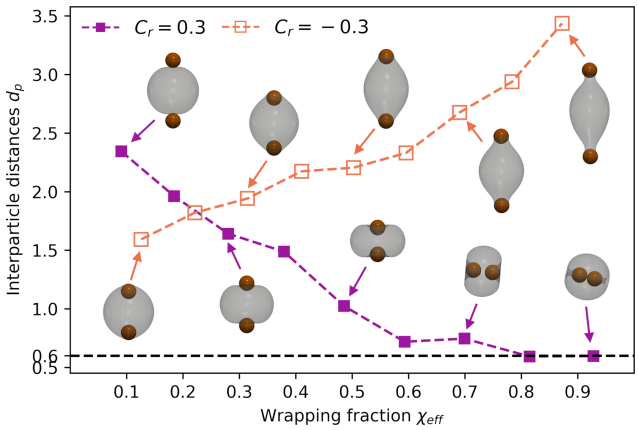

Fig. 6 Relation between particle wrapping fraction and interparticle distance for two particles of size 0.3 interacting with a vesicle simultaneously. Insets show corresponding equilibrium configurations for different wrapping states.

to a nearly spherical shape, enclosing the particles within its interior. At very high wrapping fractions, particles approach each other until contact. This close proximity can lead to changes in the vesicle topology through membrane fusion (not accounted for in this study).

3.4 Interactions of particles with biconcave-shaped vesicles

We further probe the interactions between particles and vesicles with biologically relevant shapes. Due to the extensive interest in cellular responses of nanoparticle exposure, we model biconcave discoid vesicles, which resemble healthy red blood cells (RBCs). Unlike the previous model of spherical vesicles, the biconcave vesicle is subjected to a constant volume constraint with $\kappa_v = 2.0$ to mimic a cell. Additionally, we set a target reduced volume (v) of 0.65 for the vesicle.

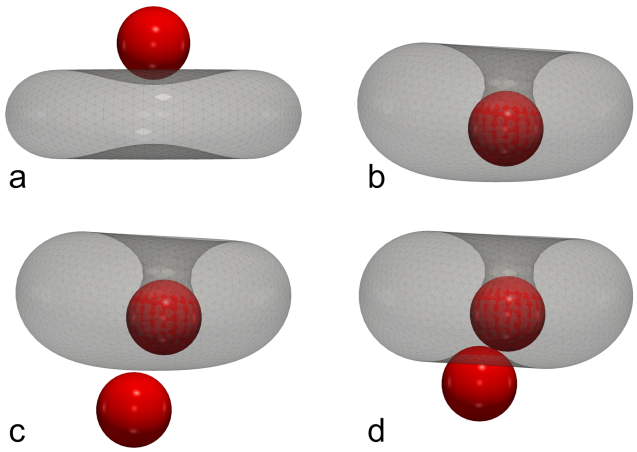

Fig. 7 (a) Initial and (b) final equilibrium snapshots of a biconcave-shaped vesicle interacting with a single particle. (c) Initial and (d) final equilibrium snapshots of the successive interaction with the second particle are also shown. Particles in red color represent spontaneous interaction with a bias potential.

We initiate our study by introducing a single particle on top of a discocyte vesicle in the concave region (Figure 7a). The interaction between the particle and vesicle occurs spontaneously without any externally imposed biasing potential. Due to the intrinsic concavity, the cell membrane naturally wraps around the particle, as shown in Movie S1. As the system reaches equilibrium, we observe an effective wrapping fraction $\chi_{eff} \approx 0.87$, confirming the successful uptake of the particle by the cell membrane (Figure 7b). After reaching the equilibrium state with the first particle, we position a second particle beneath the vesicle, again without applying any biasing potential (Figure 7c). Interestingly, the second particle achieves a considerably lower wrapping fraction of only 0.19, while the top particle maintains the same degree of wrapping. This difference in the final state is attributed to the morphological changes of the vesicle induced by the uptake of the first particle. Specifically, the lower concavity of the vesicle disappears, resulting in an unfavorable interaction between the second particle and a locally convex membrane region. In addition, the two particles come into contact after interaction with the vesicle. Figure 7(d) also illustrates the vesicle response, showing a slight shift of the top particle from the center axis. This shift can be attributed to the non-axisymmetric initial mesh configuration (see Movie S1).

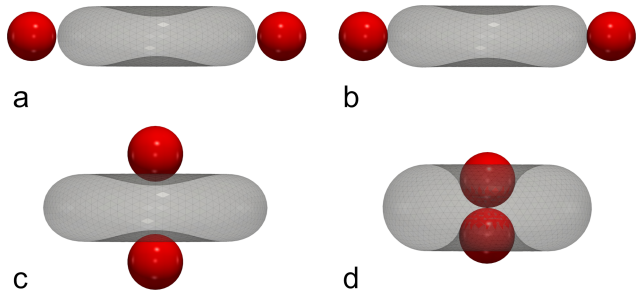

Fig. 8 (a) Initial and (b) equilibrium snapshots of the interaction between the biconcave-shaped vesicle and two particles simultaneously placed at the waist of the vesicle. (c) Initial and (b) equilibrium snapshots when the particles are initially located at the top and bottom concave regions of the vesicle. Particles in red color represent spontaneous interaction with no biasing potential.

To further investigate the effect of interaction sequence and local membrane geometry, we conduct simulations having two spherical nanoparticles simultaneously introduced to distinct regions (Figure 8). Figures 8a,b demonstrate that the vesicle fails to uptake the particles positioned at the waist due to the local convexity of the membrane. Namely, the degree of wrapping does not exceed 0.1, indicating a substantial energy barrier. In contrast, similar to the previous case, the membrane readily wraps the two particles located near the concave regions of the vesicle (Figure 8c), gradually achieving an effective wrapping fraction ≈ 0.46 for both particles, as illustrated in Figure 8d. The results underscore that the outcome of the interaction is influenced by the local membrane curvature. This behavior highlights that the concavities in the biconcave vesicle shape facilitate nanoparticle uptake and emphasizes the importance of the interaction sequence. Notably, the successful uptake of two particles would result in the contact of the membrane patches wrapping the particles (see Movie S2). We speculate that this membrane contact will lead to membrane fusion and the creation of a hole in the vesicle at the

https://doi.org/10.26434/chemrxiv-2023-wrgnr **ORCID:** https://orcid.org/0000-0002-8894-2750 Content not peer-reviewed by ChemRxiv. **License:** CC BY-NC-ND 4.0

contact point, corresponding to a topological change. This non-trivial shape transformation could disrupt the structural integrity of the cell and potentially its biological functions, or even induce wrapping-induced lysis.

Finally, we explore the dynamics of a discocyte vesicle in the presence of two strongly interacting particles positioned along its waist (see Figure 9 and Movie S3). Here, we impose the umbrella potential to enforce particle wrapping with a target wrapping fraction of 0.5. In the initial phase of the simulation (Figure 9b), we observe the vesicle elongate horizontally to facilitate particle wrapping. Consequently, the particles move apart with an increasing interparticle distance of approximately 3.76. Notably, the vesicle transitions to a dumbbell shape as a result of the particle interaction. As the simulation progresses (Figure 9c), the vesicle begins to contract, reducing d_p to approximately 2.77. Subsequently, d_p further decreases to approximately 1.96 and the two particles move toward each other along the vesicle (Figure 9d). Approaching equilibrium (Figures 9e-h), the particles aggregate toward the middle section of the vesicle, eventually coming into contact. The vesicle forms a localized dip that encapsulates both particles. Both nanoparticles achieve an effective wrapping fraction of ≈ 0.50 at the equilibrium. This result showcases the membrane-mediated nanoparticle aggregation on vesicles with complex shapes.

4 Conclusions

This study employed a force-based, continuum scale model to investigate the dynamics of fluid vesicles in response to the interactions of nanoparticles that exhibit adhesive interactions and possess dimensions greater than the membrane thickness. The membrane bending energy and total free energy profiles corresponding to the full range of wrapping fractions ($0.05 \leq \chi_{eff} \leq 0.95$) were systematically characterized for a single nanoparticle interacting with a spherical vesicle at various curvature ratios ($0.2 \leq C_r \leq 0.4$). The results demonstrate that a nanoparticle interacting from outside the vesicle must overcome a substantial energy barrier to achieve full wrapping, whereas an internal particle spontaneously attains an intermediate wrapping fraction. The particle size affects external wrapping more significantly than internal wrapping. Due to the discretization effects, the energy maxima and minima were observed at wrapping fractions higher than 0.5 predicted by the analytical theory[4]. When wrapping an extra particle, the vesicles exhibit similar energy variations, but the magnitudes of energy changes increase. The progressive wrapping of dual particles also results in opposite trends in the interparticle distance for the particles located inside or outside the vesicle. While the wrapping of internal particles drives their separation, the external particles aggregate as being wrapped more.

Furthermore, our research extends to multiple particle interactions with biological vesicles of red blood cell shapes. We elucidate the effects of initial particle positions and interaction sequences in determining the equilibrium configurations of the vesicle-particle complexes. The results show that the membrane concavity facilitates particle uptake while the convex membrane region repels adhesive particles. Vesicle shape changes induced by the interaction of the first particle influence the wrapping of ensuing particles. Finally, the simulation demonstrates highly dynamic shape variations of the biconcave vesicle when interacting with strongly adhesive particles. To conclude, this study highlights the intricacies of particle–vesicle interaction dynamics and reveals the importance of wrapping fractions and particle positioning in governing equilibrium configurations. Our results also provide insights into the potential effects of nanoparticles on biological structures.

Acknowledgements

X.Y. and K.D. gratefully acknowledge funding from the National Science Foundation for supporting this work through awards 2034855 and 2035623. Computing time was provided by the Center for Functional Nanomaterials, which is a U.S. DOE Office of Science Facility, at Brookhaven National Laboratory under contract no. DESC0012704. We would also like to acknowledge helpful discussions with Emad Pirhadi.

References

1 Amir H Bahrami, Michael Raatz, Jaime Agudo-Canalejo, Raphael Michel, Emily M Curtis, Carol K Hall, Michael Gradzielski, Reinhard Lipowsky, and Thomas R Weikl. Wrapping of nanoparticles by membranes. *Advances in colloid and interface science*, 208:214–224, 2014.

2 Amir Houshang Bahrami. Orientational changes and impaired internalization of ellipsoidal nanoparticles by vesicle membranes. *Soft Matter*, 9(36):8642–8646, 2013.

3 Amir Houshang Bahrami, Reinhard Lipowsky, and Thomas R Weikl. Tubulation and aggregation of spherical nanoparticles adsorbed on vesicles. *Physical review letters*, 109(18):188102, 2012.

4 Amir Houshang Bahrami, Reinhard Lipowsky, and Thomas R Weikl. The role of membrane curvature for the wrapping of nanoparticles. *Soft Matter*, 12(2):581–587, 2016.

5 Amir Houshang Bahrami and Thomas R Weikl. Curvature-mediated assembly of janus nanoparticles on membrane vesicles. *Nano Letters*, 18(2):1259–1263, 2018.

6 Christophe Barbe, John Bartlett, Linggen Kong, Kim Finnie, Hui Qiang Lin, Michael Larkin, Sandrine Calleja, Alexandra Bush, and Gerard Calleja. Silica particles: a novel drug-delivery system. *Advanced materials*, 16(21):1959–1966, 2004.

7 Christian Bartels and Martin Karplus. Probability distributions for complex systems: adaptive umbrella sampling of the potential energy. *The Journal of Physical Chemistry B*, 102(5):865–880, 1998.

8 Turgut Baştuğ, Po-Chia Chen, Swarna M Patra, and Serdar Kuyucak. Potential of mean force calculations of ligand binding to ion channels from jarzynski's equality and umbrella sampling. *The Journal of chemical physics*, 128(15), 2008.

9 Shahed Behzadi, Vahid Serpooshan, Wei Tao, Majd A Hamaly, Mahmoud Y Alkawareek, Erik C Dreaden, Dennis Brown, Alaaldin M Alkilany, Omid C Farokhzad, and Morteza Mahmoudi. Cellular uptake of nanoparticles: journey inside the cell. *Chemical society reviews*, 46(14):4218–4244, 2017.

https://doi.org/10.26434/chemrxiv-2023-wrgnr **ORCID:** https://orcid.org/0000-0002-8894-2750 Content not peer-reviewed by ChemRxiv. **License:** CC BY-NC-ND 4.0

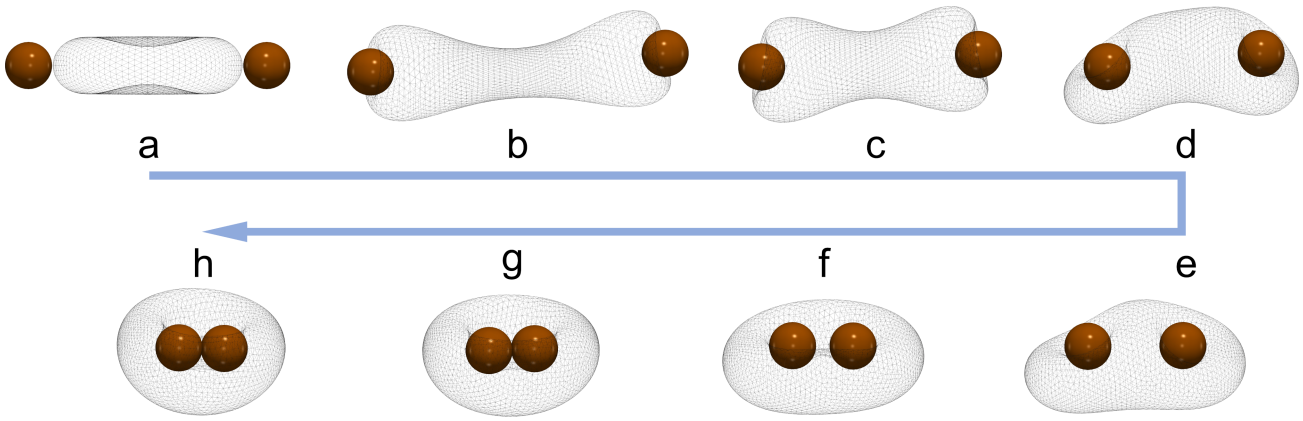

Fig. 9 Simulation snapshot sequence for interaction dynamics between two particles and the biconcave-shaped vesicle with an umbrella potential to reach target wrapping fraction of 0.5. The initial positions of the particles are on the waist. The brown color indicates the particles with the bias potential.

10 Valentina Belli, Daniela Guarnieri, Marco Biondi, Francesca Della Sala, and Paolo A Netti. Dynamics of nanoparticle diffusion and uptake in three-dimensional cell cultures. *Colloids and Surfaces B: Biointerfaces*, 149:7–15, 2017.

11 Xin Bian, Sergey Litvinov, and Petros Koumoutsakos. Bending models of lipid bilayer membranes: Spontaneous curvature and area-difference elasticity. *Computer Methods in Applied Mechanics and Engineering*, 359:112758, 2020.

12 Kenneth A Brakke. The surface evolver. *Experimental mathematics*, 1(2):141–165, 1992.

13 P. B. Canham. The minimum energy of bending as a possible explanation of the biconcave shape of the human red blood cell. *Journal of Theoretical Biology*, 26(1), 1970.

14 Leo YT Chou, Kevin Ming, and Warren CW Chan. Strategies for the intracellular delivery of nanoparticles. *Chemical society reviews*, 40(1):233–245, 2011.

15 Keenan Crane and Max Wardetzky. A glimpse into discrete differential geometry. *Notices of the American Mathematical Society*, 64(10), 2017.

16 Emily M Curtis, Amir H Bahrami, Thomas R Weikl, and Carol K Hall. Modeling nanoparticle wrapping or translocation in bilayer membranes. *Nanoscale*, 7(34):14505–14514, 2015.

17 Sabyasachi Dasgupta, Thorsten Auth, and Gerhard Gompper. Wrapping of ellipsoidal nano-particles by fluid membranes. *Soft Matter*, 9(22):5473–5482, 2013.

18 Sabyasachi Dasgupta, Thorsten Auth, and Gerhard Gompper. Shape and orientation matter for the cellular uptake of non-spherical particles. *Nano letters*, 14(2):687–693, 2014.

19 Mark E Davis, Zhuo Chen, and Dong M Shin. Nanoparticle therapeutics: an emerging treatment modality for cancer. *Nature reviews Drug discovery*, 7(9):771–782, 2008.

20 Wim H De Jong and Paul JA Borm. Drug delivery and nanoparticles: applications and hazards. *International journal of nanomedicine*, 3(2):133–149, 2008.

21 Markus Deserno. Fluid lipid membranes: From differential geometry to curvature stresses. *Chemistry and Physics of Lipids*, 185:11–45, 2015. Membrane mechanochemistry: From the molecular to the cellular scale.

22 Gary J Doherty and Harvey T McMahon. Mechanisms of endocytosis. *Annual review of biochemistry*, 78:857–902, 2009.

23 Guansheng Du, Qun Fang, and Jaap MJ den Toonder. Microfluidics for cell-based high throughput screening platforms—a review. *Analytica chimica acta*, 903:36–50, 2016.

24 Evan Evans and Yuan-Cheng Fung. Improved measurements of the erythrocyte geometry. *Microvascular research*, 4(4):335–347, 1972.

25 D Fedosov, B Caswell, and G Karniadakis. Dissipative Particle Dynamics Modeling of Red Blood Cells. pages 183–218, 6 2010.

26 Dmitry A Fedosov, Bruce Caswell, and George Em Karniadakis. A multiscale red blood cell model with accurate mechanics, rheology, and dynamics. *Biophysical journal*, 98(10):2215–2225, 2010.

27 Parisa Foroozandeh and Azlan Abdul Aziz. Insight into cellular uptake and intracellular trafficking of nanoparticles. *Nanoscale research letters*, 13:1–12, 2018.

28 Jonathan B. Freund and M. M. Orescanin. Cellular flow in a small blood vessel. *Journal of Fluid Mechanics*, 671:466–490, 3 2011.

29 Svetlana Gelperina, Kevin Kisich, Michael D Iseman, and Leonid Heifets. The potential advantages of nanoparticle drug delivery systems in chemotherapy of tuberculosis. *American journal of respiratory and critical care medicine*, 172(12):1487–1490, 2005.

30 Julien Gigault, Hind El Hadri, Brian Nguyen, Bruno Grassl, Laura Rowenczyk, Nathalie Tufenkji, Siyuan Feng, and Mark Wiesner. Nanoplastics are neither microplastics nor engineered nanoparticles. *Nature nanotechnology*, 16(5):501–507, 2021.

31 Yeongchang Goh, Yo Han Song, Gibok Lee, Hyeongyu Bae, Manoj Kumar Mahata, and Kang Taek Lee. Cellular uptake efficiency of nanoparticles investigated by three-dimensional imaging. *Physical Chemistry Chemical Physics*, 20(16):11359–11368, 2018.

https://doi.org/10.26434/chemrxiv-2023-wrgnr **ORCID:** https://orcid.org/0000-0002-8894-2750 Content not peer-reviewed by ChemRxiv. **License:** CC BY-NC-ND 4.0

32 G. Gompper and D. M. Kroll. Random surface discretization and the renormalization of the bending rigidity. *Journal de Physique I*, 6(10):1305–1320, 1996.

33 G Gompper and DM Kroll. Triangulated-surface models of fluctuating membranes. *Statistical mechanics of membranes and surfaces*, pages 359–426, 2004.

34 Eitan Grinspun, Mathieu Desbrun, Konrad Polthier, Peter Schröder, and Ari Stern. Discrete differential geometry: an applied introduction. *ACM Siggraph Course*, 7(1), 2006.

35 Wolfgang Helfrich. Elastic properties of lipid bilayers: theory and possible experiments. *Zeitschrift für Naturforschung c*, 28(11-12):693–703, 1973.

36 Peter HM Hoet, Irene Brüske-Hohlfeld, and Oleg V Salata. Nanoparticles–known and unknown health risks. *Journal of nanobiotechnology*, 2:1–15, 2004.

37 Timon Idema and Daniela J Kraft. Interactions between model inclusions on closed lipid bilayer membranes. *Current Opinion in Colloid & Interface Science*, 40:58–69, 2019.

38 Alec Jacobson, Daniele Panozzo, et al. libigl: A simple C++ geometry processing library, 2018. https://libigl.github.io/.

39 Shuangshuang Jin, Robert R Lewis, and David West. A comparison of algorithms for vertex normal computation. *The visual computer*, 21:71–82, 2005.

40 Jichul Kim. A review of continuum mechanics for mechanical deformation of lipid membranes. *Membranes*, 13(5):493, 2023.

41 PB Sunil Kumar, Gerhard Gompper, and Reinhard Lipowsky. Budding dynamics of multicomponent membranes. *Physical review letters*, 86(17):3911, 2001.

42 Aymen Laadhari, Chaouqi Misbah, and Pierre Saramito. On the equilibrium equation for a generalized biological membrane energy by using a shape optimization approach. *Physica D: Nonlinear Phenomena*, 239(16):1567–1572, 2010.

43 Pascale R Leroueil, Seungpyo Hong, Almut Mecke, James R Baker Jr, Bradford G Orr, and Mark M Banaszak Holl. Nanoparticle interaction with biological membranes: does nanotechnology present a janus face? *Accounts of chemical research*, 40(5):335–342, 2007.

44 Xuefei Lu, Ying Liu, Xiangjun Kong, Peter E Lobie, Chunying Chen, and Tao Zhu. Nanotoxicity: a growing need for study in the endocrine system. *Small*, 9(9-10):1654–1671, 2013.

45 Bryce J Marquis, Sara A Love, Katherine L Braun, and Christy L Haynes. Analytical methods to assess nanoparticle toxicity. *Analyst*, 134(3):425–439, 2009.

46 Mark Meyer, Mathieu Desbrun, Peter Schröder, and Alan H Barr. Discrete differential-geometry operators for triangulated 2-manifolds. In *Visualization and mathematics III*, pages 35–57. Springer, 2003.

47 Mark Meyer, Mathieu Desbrun, Peter Schröder, and Alan H. Barr. Discrete Differential-Geometry Operators for Triangulated 2-Manifolds. pages 35–57, 2003.

48 Hiroshi Noguchi. Membrane simulation models from nanometer to micrometer scale. *Journal of the Physical Society of Japan*, 78(4):041007, 2009.

49 Hiroshi Noguchi and Gerhard Gompper. Fluid vesicles with viscous membranes in shear flow. *Physical review letters*, 93(25):258102, 2004.

50 Hiroshi Noguchi and Gerhard Gompper. Fluid vesicles with viscous membranes in shear flow. *Physical Review Letters*, 93(25), 12 2004.

51 Günter Oberdörster, Eva Oberdörster, and Jan Oberdörster. Nanotoxicology: an emerging discipline evolving from studies of ultrafine particles. *Environmental health perspectives*, 113(7):823–839, 2005.

52 Weria Pezeshkian and Siewert J Marrink. Simulating realistic membrane shapes. *Current opinion in cell biology*, 71:103–111, 2021.

53 Michael Raatz, Reinhard Lipowsky, and Thomas R Weikl. Cooperative wrapping of nanoparticles by membrane tubes. *Soft Matter*, 10(20):3570–3577, 2014.

54 Michael Raatz and Thomas R Weikl. Membrane tubulation by elongated and patchy nanoparticles. *Advanced Materials Interfaces*, 4(1):1600325, 2017.

55 Pia L Rodriguez, Takamasa Harada, David A Christian, Diego A Pantano, Richard K Tsai, and Dennis E Discher. Minimal" self" peptides that inhibit phagocytic clearance and enhance delivery of nanoparticles. *Science*, 339(6122):971–975, 2013.

56 Raj Kumar Sadhu, Sarah R. Barger, Samo Penič, Aleš Iglič, Mira Krendel, Nils C. Gauthier, and Nir S. Gov. A theoretical model of efficient phagocytosis driven by curved membrane proteins and active cytoskeleton forces. *Soft Matter*, 19:31–43, 2023.

57 Gaurav Sahay, Daria Y Alakhova, and Alexander V Kabanov. Endocytosis of nanomedicines. *Journal of controlled release*, 145(3):182–195, 2010.

58 Ramin Sakhtianchi, Rodney F Minchin, Ki-Bum Lee, Alaaldin M Alkilany, Vahid Serpooshan, and Morteza Mahmoudi. Exocytosis of nanoparticles from cells: role in cellular retention and toxicity. *Advances in colloid and interface science*, 201:18–29, 2013.

59 Isaac Salib, Xin Yong, Emily J Crabb, Nicholas M Moellers, Gerald T McFarlin IV, Olga Kuksenok, and Anna C Balazs. Harnessing fluid-driven vesicles to pick up and drop off janus particles. *ACS nano*, 7(2):1224–1238, 2013.

60 Anđela Šarić and Angelo Cacciuto. Mechanism of membrane tube formation induced by adhesive nanocomponents. *Physical review letters*, 109(18):188101, 2012.

61 H Bernhard Schlegel. Geometry optimization. *Wiley Interdisciplinary Reviews: Computational Molecular Science*, 1(5):790–809, 2011.

62 T Seifert, O Zschörnig, J Arnhold, and K Arnold. Beta-blockers inhibit the modification of low-density lipoproteins by sodium hypochlorite in vitro. *Chemistry and physics of lipids*, 85(1):13–21, 1997.

63 Udo Seifert, Karin Berndl, and Reinhard Lipowsky. Shape transformations of vesicles: Phase diagram for spontaneous-curvature and bilayer-coupling models. *Physical review A*, 44(2):1182, 1991.

https://doi.org/10.26434/chemrxiv-2023-wrgnr **ORCID:** https://orcid.org/0000-0002-8894-2750 Content not peer-reviewed by ChemRxiv. **License:** CC BY-NC-ND 4.0

64 Marc Siggel, Sebastian Kehl, Klaus Reuter, Jürgen Köfinger, and Gerhard Hummer. Trimem: A parallelized hybrid monte carlo software for efficient simulations of lipid membranes. *The Journal of Chemical Physics*, 157(17):174801, 2022.

65 Rajesh Singh and James W Lillard Jr. Nanoparticle-based targeted drug delivery. *Experimental and molecular pathology*, 86(3):215–223, 2009.

66 Kushal Sinha and Michael D Graham. Dynamics of a single red blood cell in simple shear flow. *Physical Review E*, 92(4):042710, 2015.

67 David Steigmann. Fluid films with curvature elasticity. *Archive for Rational Mechanics and Analysis*, 150(2):127–152, 1999.

68 Robert Vácha, Francisco J Martinez-Veracoechea, and Daan Frenkel. Receptor-mediated endocytosis of nanoparticles of various shapes. *Nano letters*, 11(12):5391–5395, 2011.

69 Françoise M Winnik and Dusica Maysinger. Quantum dot cytotoxicity and ways to reduce it. *Accounts of chemical research*, 46(3):672–680, 2013.

70 Yan Xiao, Samuel P Forry, Xiugong Gao, R David Holbrook, William G Telford, and Alessandro Tona. Dynamics and mechanisms of quantum dot nanoparticle cellular uptake. *Journal of Nanobiotechnology*, 8(1):1–9, 2010.

71 Kai Xiong, Jiayin Zhao, Daowen Yang, Qingwen Cheng, Jiuling Wang, and Hongbing Ji. Cooperative wrapping of nanoparticles of various sizes and shapes by lipid membranes. *Soft Matter*, 13(26):4644–4652, 2017.

72 Xin Yong, Emily J Crabb, Nicholas M Moellers, and Anna C Balazs. Self-healing vesicles deposit lipid-coated janus particles into nanoscopic trenches. *Langmuir*, 29(52):16066–16074, 2013.

73 Xin Yong and Ke Du. Effects of shape on interaction dynamics of tetrahedral nanoplastics and the cell membrane. *The Journal of Physical Chemistry B*, 127(7):1652–1663, 2023.

74 Qingfen Yu, Sabyasachi Dasgupta, Thorsten Auth, and Gerhard Gompper. Osmotic concentration-controlled particle uptake and wrapping-induced lysis of cells and vesicles. *Nano letters*, 20(3):1662–1668, 2020.

75 Qingfen Yu, Sameh Othman, Sabyasachi Dasgupta, Thorsten Auth, and Gerhard Gompper. Nanoparticle wrapping at small non-spherical vesicles: curvatures at play. *Nanoscale*, 10(14):6445–6458, 2018.

76 Christopher D Zangmeister, James G Radney, Kurt D Benkstein, and Berc Kalanyan. Common single-use consumer plastic products release trillions of sub-100 nm nanoparticles per liter into water during normal use. *Environmental Science & Technology*, 56(9):5448–5455, 2022.

77 Sulin Zhang, Ju Li, George Lykotrafitis, Gang Bao, and Subra Suresh. Size-dependent endocytosis of nanoparticles. *Advanced materials (Deerfield Beach, Fla.)*, 21:419, 2009.

78 Feng Zhao, Ying Zhao, Ying Liu, Xueling Chang, Chunying Chen, and Yuliang Zhao. Cellular uptake, intracellular trafficking, and cytotoxicity of nanomaterials. *small*, 7(10):1322–1337, 2011.

79 Ou-Yang Zhong-Can and Wolfgang Helfrich. Bending energy of vesicle membranes: General expressions for the first, second, and third variation of the shape energy and applications to spheres and cylinders. *Physical Review A*, 39(10):5280, 1989.

80 Wenting Zhou, Jian Le, Yang Chen, Ying Cai, Zhanying Hong, and Yifeng Chai. Recent advances in microfluidic devices for bacteria and fungus research. *TrAC Trends in Analytical Chemistry*, 112:175–195, 2019.

81 Cuncheng Zhu, Christopher T Lee, and Padmini Rangamani. Mem3dg: modeling membrane mechanochemical dynamics in 3d using discrete differential geometry. *Biophysical reports*, 2(3):100062, 2022.

https://doi.org/10.26434/chemrxiv-2023-wrgnr **ORCID:** https://orcid.org/0000-0002-8894-2750 Content not peer-reviewed by ChemRxiv. **License:** CC BY-NC-ND 4.0